

## Noninvasive real time tomographic imaging of epileptic foci and networks

Liangzhong Xiang<sup>a</sup>, Lijun Ji<sup>a</sup>, Tao Zhang<sup>a</sup>, Bo Wang<sup>a</sup>, Jianjun Yang<sup>a</sup>, Qizhi Zhang<sup>a</sup>, Max S. Jiang<sup>a</sup>, Junli Zhou<sup>b,c</sup>, Paul R. Carney<sup>a,b,c,d</sup>, Huabei Jiang<sup>a,\*</sup>

<sup>a</sup> J. Crayton Pruitt Family Department of Biomedical Engineering, University of Florida, Gainesville, FL 32611, USA

<sup>b</sup> Departments of Pediatrics, Neurology, and Neuroscience, University of Florida, Gainesville, FL 32611, USA

<sup>c</sup> Wilder Center of Excellence for Epilepsy Research, University of Florida, Gainesville, FL 32611, USA

<sup>d</sup> McKnight Brain Institute, University of Florida, Gainesville, FL 32611, USA

### ARTICLE INFO

#### Article history:

Accepted 25 October 2012

Available online 2 November 2012

#### Keywords:

Real time photoacoustic tomography (PAT)

Noninvasive seizure dynamic imaging

Epileptic foci and networks

Pre-surgical planning

### ABSTRACT

While brain imaging and electrophysiology play a central role in neuroscience research and in the evaluation of neurological disorders, a single noninvasive modality that offers both high spatial and temporal resolution is currently not available. Here we show in an acute epilepsy rat model that photoacoustic tomography (PAT) can noninvasively track seizure brain dynamics with both high spatial and temporal resolution, and at a depth that is clinically relevant. The noninvasive yet whole surface and depth capabilities of the PAT system allowed us to actually see what is happening during ictogenesis in terms of seizure onset and spread. Both seizure onset and propagation were tomographically detected at a spatial resolution of 150  $\mu\text{m}$  and a temporal resolution of 300 ms, respectively. The current study lends support to the theory that seizure onset and spread involves a rich interplay between multiple cortical and subcortical brain areas during the onset and spread of epileptic seizures. Dynamical changes of vasculature during epileptiform events were also detected with high spatiotemporal resolution. Together, these findings suggest that PAT represents a powerful tool for noninvasively mapping seizure onset and propagation patterns, and the 'functional' connectivity within epileptic brain networks.

© 2012 Elsevier Inc. All rights reserved.

### Introduction

Epilepsy is a common, chronic, neurological disorder characterized by seizures. Three percent of people will be diagnosed with epilepsy at some time in their lives (Hauser et al., 1996). Indeed, approximately 50 million people worldwide have epilepsy, and 20 to 30% of these patients are refractory to all forms of medical treatment (Hauser, 1992). In most cases, seizures are controlled, although not cured, with anticonvulsant medication. Seizure types are classified according to whether the source of the seizure is localized (partial or focal onset seizures) or distributed (generalized seizures) (Greenfield et al., 2011). Localization-related epilepsies arise from an epileptic focus. A partial seizure may spread within the brain, a process known as secondary generalization. Generalized epilepsies, in contrast, arise from many independent foci (multifocal epilepsies) or from epileptic circuits that involve the whole brain. In epilepsies of unknown localization, it remains unclear as to whether they arise from a portion of the brain or from more widespread circuits.

For those patients with medically intractable focal epilepsy, the best treatment option is resective brain surgery (Berg et al., 2007; Birbeck et al., 2002; Duncan et al., 2006). Although several factors can impact the success of epilepsy surgery, the primary reason of failure is the incomplete mapping of the local epilepsy network which results in incomplete resection of epileptogenic foci (Engel, 2004; Jeha et al., 2007). Much of the attention on epilepsy surgery has been directed at identifying single neuronal populations. This approach has, in many cases, led to failed surgical outcomes, because seizures typically involve groups of neurons interacting both locally and across several cortical and subcortical brain regions. A better understanding of the regional interactions occurring at the site of seizure onset and spread may provide important insights about the pathophysiology of seizures and aid with accurate brain mapping and resection of the epileptic focus.

In theory, removing the focus should result in a patient's seizures being cured. However, there is much evidence to suggest that the focus is more of a region of seizure onset with a number of sites that can act independently to initiate seizures (Thom et al., 2010a, b). Seizures in animal models and in people often have a multifocal or broadly synchronized onset. The best evidence for multifocality within the seizure onset zone comes from surgical experience with intracranial monitoring. The challenge of mapping the epileptic focus stems from the observation that the pathology associated with focal epilepsy is often distributed across a number of brain sites

\* Corresponding author at: University of Florida College of Engineering, J. Crayton Pruitt Family Department of Biomedical Engineering, JG56 BMS Building, Gainesville, FL 32611, USA.

E-mail address: [hjiang@bme.ufl.edu](mailto:hjiang@bme.ufl.edu) (H. Jiang).

(Bertram, 2009) and that current diagnostics methods frequently fall short of identifying such sites. Animal studies indicate that the neurons involved in the epileptic circuitry have enhanced excitability throughout (Bertram et al., 1998; Fountain et al., 1998; Mangan et al., 2000). The implication of these observations is that each of the sites could act independently to initiate a seizure or, potentially, to drive another site into a seizure. Thus, in focal epilepsy, one may view a cortical region as a broad seizure onset zone, with the potential that multiple foci can act as a seizure focus for any given seizure.

Much of our understanding about focal seizure circuitry comes from electrophysiological recording methods. Although electrophysiology is currently the ‘gold standard’ in mapping the epileptic focus, it is often inadequate to define the boundary of the epilepsy circuitry due to spatial sampling limitations and volume conduction. What we truly desire is a brain mapping modality, which could give a high-resolution real time spatial and temporal ‘read out’ of the dynamics of cortical processing and seizures. It has been well established that optical contrast is highly sensitive to neuronal activity (Grinvald et al., 1988; Hill and Keynes, 1949). The high optical contrast is largely due to the changes in blood volume and blood oxygenation, both of which substantially increase during seizures, and increase in oxygenation metabolic rate results in increased demands on autoregulatory mechanisms (Folbergrová et al., 1981). Taking the advantage of the oxygenation dependence in the optical absorption spectrum of hemoglobin, optical imaging or intrinsic optical signal (IOS) methodologies have provided excellent surface maps of epileptic focus (Haglund and Hochman, 2004; Haglund et al., 1992). Although near-infrared spectroscopy (NIRS) (Steinhoff et al., 1996; Sokol et al., 2000; Watanabe et al., 2000) and blood-oxygen-level-dependent (BOLD) MRI can assess oxygen saturation with endogenous contrasts, BOLD MRI is sensitive only to HbR with low temporal resolution (Ogawa et al., 1990). In addition, the major limitation of NIRS and IOS is that each provides only surface depth information. Greater depth information can be obtained by using tomographic reconstruction methods such as diffuse optical tomography (Bluestone et al., 2001; Boas et al., 2001; Jiang et al., 1996; O’Leary et al., 1995). Whereas diffuse optical tomography has low spatial resolution, laser-induced photoacoustic tomography (PAT) has both superior spatial and temporal resolution. PAT detects absorbed photons ultrasonically by employing the photoacoustic effect. It combines both high contrast and spectroscopic specificity based on the optical absorption of both oxy- and deoxy-hemoglobin with high ultrasonic spatial resolution (Kruger and Liu, 1994; Laufer et al., 2007; Xiang et al., 2007; Yuan et al., 2007). Relative to other optical imaging modalities, PAT has the advantage of mitigating both scalp and skull light scattering by a factor of ~1000. The end result is that PAT allows for high spatial resolution imaging of brain at a depth considerably beyond the soft depth limit of conventional optical imaging techniques such as confocal microscopy (Sipkins et al., 2005), two-photon microscopy (Denk et al., 1990), and optical coherence tomography (Huang et al., 1991). The strong preferential optical absorption of hemoglobin makes PA imaging to have a better imaging contrast than ultrasound (US); as it can be difficult to visualize the microvessels with pulse-echo US owing to the weak echogenicity (Mace et al., 2011).

In this study, PAT was employed to image seizures in an experimental acute bicuculline methiodide model of focal epilepsy. Bicuculline is a light-sensitive competitive antagonist of GABA<sub>A</sub> receptors that mimics focal epilepsy when applied to brain tissue. During focal application of bicuculline into the brain cortex, brains were imaged noninvasively with a novel PAT system that has three orders of magnitude higher temporal resolution and four-fold higher spatial resolution relative to our previous PAT prototype (Zhang et al., 2008). Off-line, we employed measures of brain connectivity to further identify the functional anatomy implicated in focal cortical seizures. The high spatial and temporal sampling of the novel PAT system allowed for the first time the complete mapping of an epileptiform event *in vivo*.

## Methods

### Animals

Male Sprague–Dawley rats (Harlan Labs, Indianapolis, IN) weighing 50–60 g on arrival were allowed one week to acclimate to the 12-h light/dark cycle and given food and water ad libitum. All procedures were approved by the University of Florida Animal Care and Use Committee and conducted in accordance with the National Institutes of Health Guide for the Care and Use of Experimental Animals.

### PAT imaging

Light from a Ti: Sapphire laser tunable (690 to 950 nm) was delivered through the skull to the brain through an optical fiber (Fig. 1a). The energy of each laser pulse was detected by a photodiode for calibration. A 192 element full-ring transducer array was used to capture the photoacoustic (PA) signals generated by the laser light. The 192 channel data acquisition system consisted of preamplifiers, secondary stage amplifiers (for optimizing the signal-to-noise ratio), and a 3:1 electronic multiplexer coupled with a 64-channel analog-to-digital converter. Each ultrasonic detector had a 5-MHz central frequency and a 70% nominal bandwidth with a diameter of 6 mm (Blatek, Inc., PA, USA).

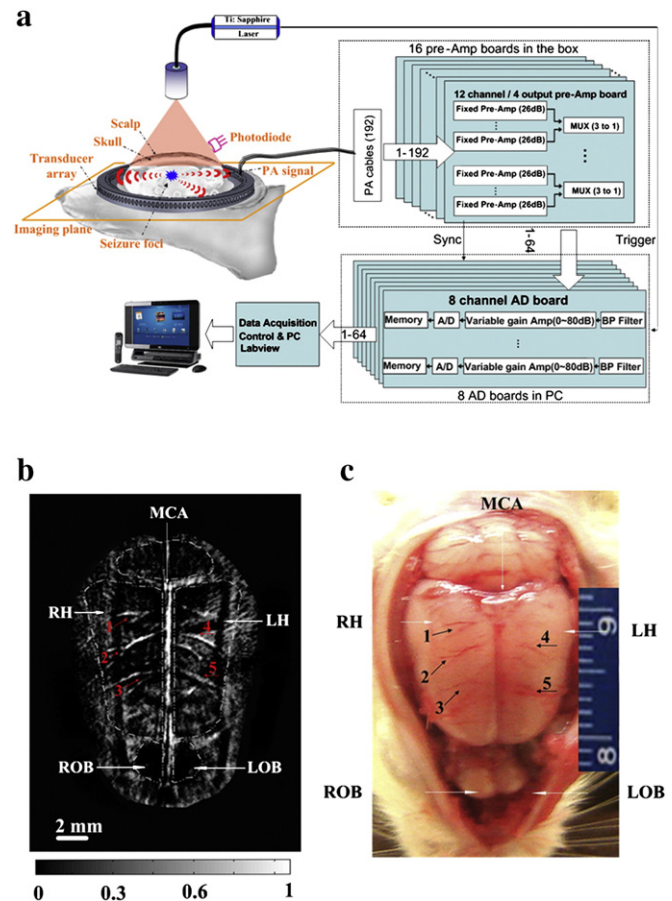


**Fig. 1.** Real time PAT system for seizure dynamics. (a.) Schematic of the real time PAT system. A 192-element full-ring transducer array was used to capture the PA signal during seizure onset. (b.) Noninvasive PAT imaging of a rat brain *in vivo* with the skin and skull intact. MCA, middle cerebral artery; RH, right hemispheres; LH, left hemispheres; LOB, left olfactory bulbs; ROB, Right olfactory bulbs. (c.) Open-skull photograph of the rat brain surface acquired after the PAT experiment. Numbers 1–5 indicate the corresponding blood vessels in the PAT image and rat brain photograph.

## Electrode implantation surgery

Animals were anesthetized intraperitoneally with 1 g/kg of body weight dose of urethane. Two 300  $\mu\text{m}$  diameter stainless steel screw electrodes were implanted within the skull for obtaining subdural multichannel cortical local field potentials data ( $-0.3$  mm posterior, 3 mm lateral (right) of bregma, 1 mm ventral) based on coordinates from a rat brain atlas (Paxinos, 1998). One, 300  $\mu\text{m}$  diameter stainless steel screw electrode (FHC, Bowdoin, ME) was implanted as a reference electrode into the midline occipital bone. Cortical local field potentials were obtained using a Tucker Davis Pentusa (Tucker Davis Technologies, Alachua, FL) neural recording system at 12 kHz, digitized with 16 bits of resolution, and band pass filtered from 0.5 to 6 kHz.

## Induction of seizures

Rats ( $n=10$ ) received 10  $\mu\text{l}$  of 1.9 mM bicuculline methiodide and 10  $\mu\text{l}$  normal saline into the left and right parietal cortex, respectively. The infusion was performed through the previously implanted electrode sites at a rate of 0.3  $\mu\text{l}/\text{min}$ . The infusion system consisted of a 100  $\mu\text{l}$  gas-tight syringe (Hamilton, Reno, NV) driven by a syringe pump (Cole-Parmer, Vernon Hills, IL) connected to polyaryletheretherketone (PEEK) tubing (ID = 0.381 mm, OD = 0.794 mm, length  $\sim 0.5$  m, Upchurch Scientific, Oak Harbor, WA). The PEEK tubing was coupled to a silica cannula (ID = 50  $\mu\text{m}$ , OD = 147  $\mu\text{m}$ , Polymicro Technologies, Phoenix, AZ) via a microfluidic connector. Cortical local field potentials were recorded 5 min before each injection and continued for up to 30 min thereafter.

## Image analysis

A custom software utility was written and incorporated into the computer software package MATLAB (MathWorks, Massachusetts, USA) to analyze and display recorded data. This software enabled the reconstruction of the PAT images and the determination of the blood vessel diameter. Amira (version 5.3.3, TGS Template Graphics Software) was used for three-dimensional reconstruction of the seizure foci. We used the frequency domain Granger causality methodology to evaluate the dynamic interactions within the seizure circuitry and the associated brain networks (Brovelli et al., 2004; Granger, 1969; Wang et al., 2007). The time-series data were selected from 200 sets of PAT images sampled at 3 Hz within the seizure onset period, and at each time point, we chose 9 (regions of interest) ROI (R1–R9) and then the PA signal was averaged within each ROI, as shown in Fig. 5b1. Changes in photoacoustic signals were quantified as  $-\Delta A/A$  in Fig. 5b3, right. The PA data shown in Figs. 3–5 were not averaged. The image color scale was determined by the photoacoustic signal intensity in arbitrary units (between 0 and 1).

## Results

### Noninvasive epileptic foci localization

Temporal and spatial resolutions of the PAT system were experimentally determined. PA images depicting frames from a 10-second sequence of dynamic ink flow through a 0.3 mm diameter tube was shown in Movie S1. The movie shows that the temporal resolution of this imaging system was  $\sim 0.33$  s/frame. Cross-sectional PA image of a two-copper-rods phantom was used to test the spatial resolution of the PAT imaging system. The two copper rods (diameter: 0.05 mm) were embedded in a cylindrical tissue-mimicking phantom at a depth of 10 mm. The center-to-center distance between the two copper rods was approximately 2.2 mm. The spatial resolution of the imaging system calculated with Rayleigh's law was 150  $\mu\text{m}$ . The spatial

resolution of the PAT system was inversely related to the bandwidth of the ultrasonic transducer.

The noninvasive PAT image of the rat cortical vasculature (Fig. 1b) matched well with an anatomical atlas (Paxinos, 1998) (Fig. 1c) obtained after the PA imaging. The brain structures including the middle cerebral artery, right hemispheres, left hemispheres, left olfactory bulbs, and right olfactory bulbs are clearly shown in the PAT image. Numbers 1–5 marked in the image indicate that the micro-blood vessels with a diameter of less than 100  $\mu\text{m}$  are also seen, which again correspond well with the rat brain photograph. This allowed for imaging objects of 50  $\mu\text{m}$  in diameter with a spatial resolution of 150  $\mu\text{m}$  (Figs. 2b, c).

Thirty minutes following the microelectrode placement, PAT imaging was performed to generate baseline tissue absorption maps, visualize micro blood vessels, and morphological cortical landmarks (Figs 3b, c). Subsequently, rats ( $n=10$ ) received 10  $\mu\text{l}$  of 1.9 mM bicuculline methiodide and 10  $\mu\text{l}$  normal saline into the left [ $-1.0\text{AP}$ , 2.5ML, 2.4DV] and right [ $-1.0\text{AP}$ , 2.5 ML, 0.4DV] parietal cortex, respectively, based on coordinates from a rat brain atlas (Paxinos, 1998). Immediately following the focal infusions, PAT imaging was repeated to visualize changes in the injection site tissue absorption. An increase in tissue absorption was observed in the bicuculline methiodide cortical injection site and surrounding region (Fig. 3c, left), but not in the saline injection site or surrounding region (Fig. 3c, right). PAT scanning for subcortical changes was also performed. Slices 5, 7, and 9 (Fig. 3d) are the images obtained 3, 5 and 7 mm below the scalp, respectively. Fig. 3e is the three dimensional rendering of the epileptic foci obtained from different tomographic layers (movie S2). Each image exhibited the variable patterns of seizure onset and propagation both at the cortical and subcortical regions. Seizures were confirmed by concomitant time-locked PAT/video-electroencephalography (Fig. 3a). Experiments were repeated for each animal at 2-hour intervals.

### Real time monitoring of epileptic events

Epileptiform events were recorded with PAT from a focal region of interest of  $\sim 2 \times 3$  mm (Fig. 4a). We observed a significant optical absorption change directly associated with de-oxygenation at a wavelength of 755 nm (Fig. 4c). Furthermore, at the seizure onset at 1 min 6.267 s, the seizure focus measured 0.2053  $\text{mm}^2$  and increased to 0.5004  $\text{mm}^2$  as the electrographic seizure time-series increased in frequency and amplitude (Fig. 4b). Corresponding rate changes (0.33 s) spike and wave discharges and PA images were observed in each experimental trial. The seizure onset dynamics captured photoacoustically are best appreciated in movies displaying how the seizure was generated and varied over time (Movie S3). PAT images suggest that in addition to ictal spread from the primary focus, homotopic foci are seen in the contralateral parietal cortex (Fig. 5a1–4). The PA signal in the contralateral foci was smaller in magnitude and delayed in time compared to the signal recorded from the primary seizure foci. We also observed a region of inverted optical signal immediately surrounding the seizure onset zone (Fig. 5b2–3). We performed analysis of the optical signal at a distance of at least 2 mm ( $\pm 0.01$ ) away from the edge of the focus. Our results demonstrate that the photoacoustic signal was inversely related to the optical signal recorded from the focus (Fig. 5b3).

To evaluate the dynamic interactions within the seizure circuitry and capture the associated networks we used the frequency domain Granger causality (Brovelli et al., 2004; Granger, 1969; Wang et al., 2007). PAT time series data was selected from 200 sets of PAT images sampled at 3 Hz within the seizure onset period. At each time point we chose 9 ROIs (Fig. 5b1) and used the averaged optical absorption within each region for the network analysis. Nine sets of time series analysis were classified into 3 groups including the primary ictal onset area and corresponding 4 surrounding regions of interest including the primary or initiating seizure focus, contralateral homotopic foci, and 2 regions of interest surrounding the primary focus in the

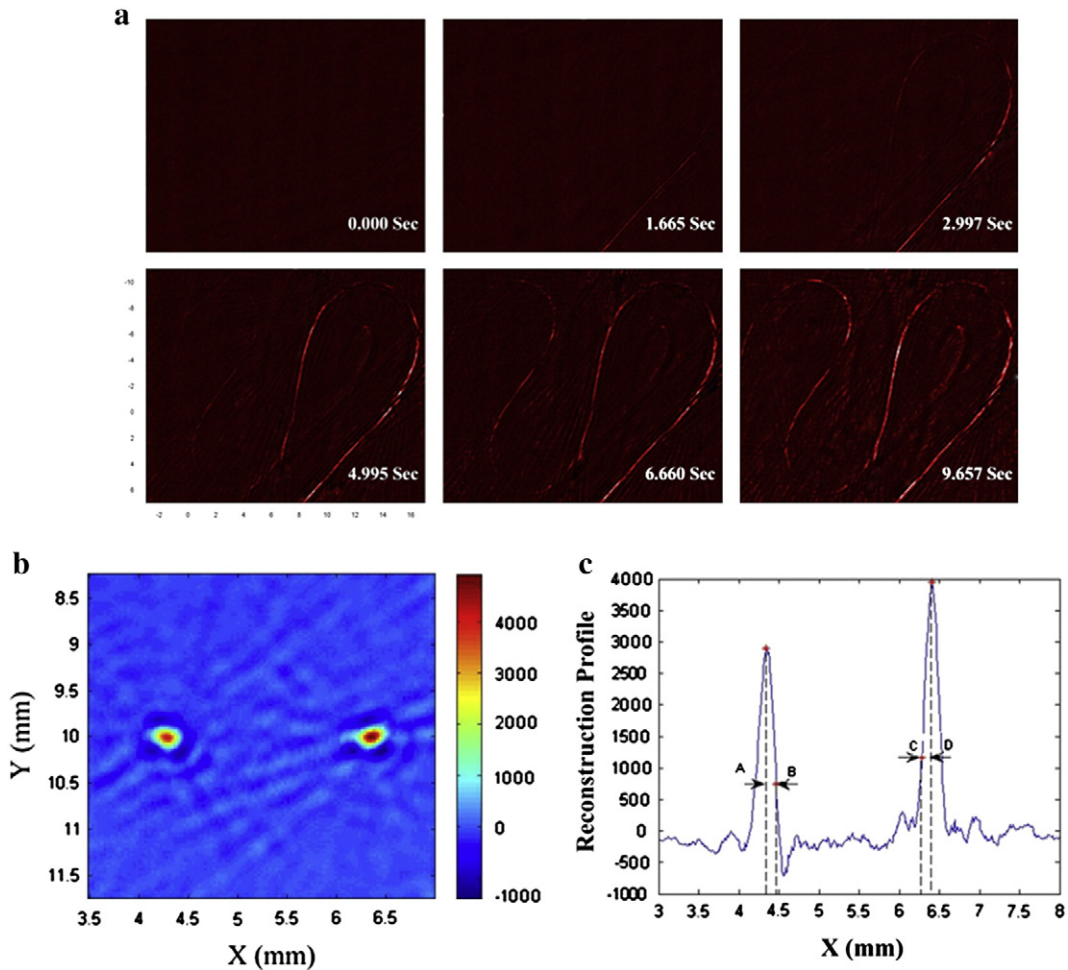


**Fig. 2.** Temporal and spatial resolution demonstration of the PAT system. (a.) Temporal resolution demonstration of the PAT system. Photoacoustic images depicting frames from a 10-second sequence of dynamic ink flow through a 0.3 mm diameter tube (Movie S1). The movie shows that the temporal resolution of this imaging system was  $\sim 0.33$  s/frame. (b.) Cross-sectional PA image of a two-copper-rods phantom. The two copper rods (diameter: 0.05 mm) were embedded in a cylindrical tissue-mimicking phantom at a depth of 10 mm. The center-to-center distance between the two copper rods was approximately 2.2 mm. (c.) The normalized profile of the reconstructed PA image shown in (b.) along  $y = 10$  mm. The half- and quarter-amplitude widths were obtained by measuring the distance between points AB and between CD, respectively. The spatial resolution of the imaging system calculated with Rayleigh's law was  $150 \mu\text{m}$ .

contralateral cortex. The middle cerebral artery, primary seizure focus, and secondary homotopic seizure focus were also analyzed. Results from group 1 analysis demonstrate the causal influence from the primary focus to the surrounding regions of interest (Fig. 5b1). The negative zero-lag correlation ( $-0.68$ ) between both the primary and secondary foci showed that neural activities within these two regions changed in opposite direction over time. Fig. 5b4 shows the Granger causality analysis for group 2 data where we see that the primary and secondary contralateral brain foci influenced each other mutually with a stronger influence of the primary focus relative to the contralateral focus. Moreover, we suggest that the primary seizure focus may influence the contralateral foci as previously suggested using optical intrinsic imaging in epilepsy (Khalilov et al., 2003) and microelectrode recordings of hippocampus local field potentials (Cadotte et al., 2010). Finally, from group 3 analyses (Fig. 5b5) we found that the primary focus strongly influenced the hemodynamic change in the middle cerebral artery, which in turn showed influence on the contralateral homotopic foci.

#### *Dynamical changes of vasculature during interictal discharges*

Fig. 6a shows image of the rat cortex vasculature through the intact scalp and skull. The red arrow indicates the microvasculature along the direction marked by the yellow dashed line, representing a cross-sectional scanning using a 50 MHz ultrasound transducer. Positive and negative acoustic peaks induced by a  $25 \mu\text{m}$  blood vessel

were sorted out as target signals to track the change of the vessel diameter. Typical PA signals from the targeted vessel at different times show apparent vessel vasomotion by  $\sim 40\%$  (mean = 40%,  $P < 0.03$ ,  $N = 20$ ) during the interictal discharges (Fig. 6b). Local field potential recordings (Fig. 6c) showed that interictal spikes had a strong correlation with the discrete change in vessel size observed photoacoustically (Fig. 6d; error bars  $\pm$  s.d. was calculated from 20 consecutive spikes).

#### **Discussion**

The main finding is that PAT imaging is a novel tool for noninvasively mapping seizure dynamics with both high spatial and temporal resolution. This study investigated the hemodynamic changes during focal seizure onset and propagation in an acute model of focal epilepsy. The experimental results suggest that the increase in local and surrounding brain tissue absorption was due to the focal bicuculline methiodide induced seizure rather than other factors such as stab cortex tissue wound injection. Epileptiform events, including interictal spikes, ictal onset and spread were identified in near real time. To the best of our knowledge, this is the first experimental evidence for millisecond temporal resolution, centimeters depth, and micron scale imaging of focal seizure onset and spread by a noninvasive technique.

Quantitative photoacoustic image reconstruction can be used to resolve the light scattering problem with the deeper penetration in

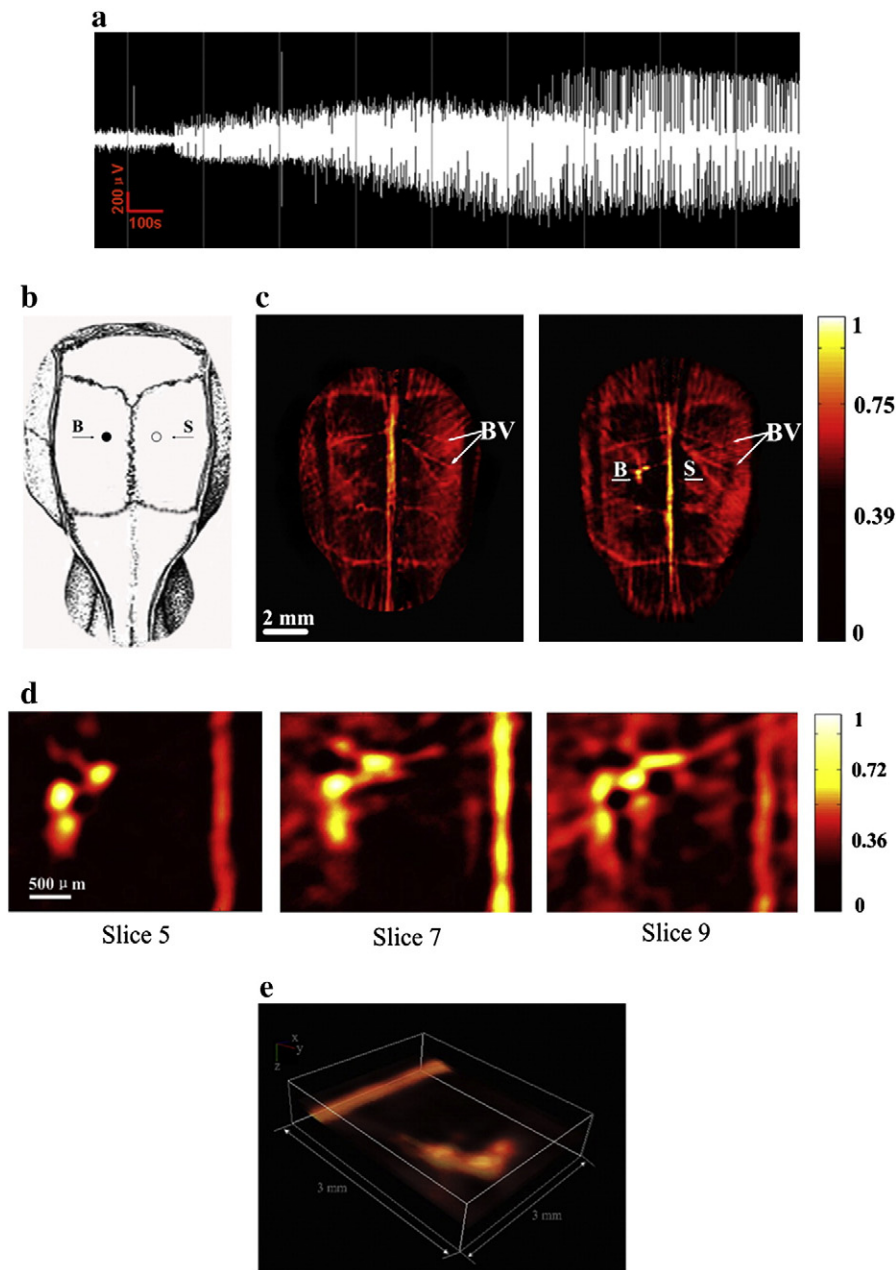


**Fig. 3.** Noninvasive epileptic foci localization. (a.) EEG recordings of seizure onset after BMI injection. (b.) Schematic showing the location of BMI injection and saline injection (control). B, BMI injection; S, saline injection. (c.) Reconstructed PAT image before (left) and after (right) the BMI injection. The BMI and saline were injected into the left and right parietal neocortex, respectively. A significant increase of optical absorption is seen in the region of the BMI injection, while no absorption contrast is observed in the region of the saline injection relative to its surroundings. (d.) Series of PAT images from three representative transverse planes parallel to the skin surface with 755 nm wavelength. Slices 5, 7, and 9 are the images obtained 3, 5 and 7 mm under the skin, respectively. The images show different spatial patterns at the seizure foci at different tomographic layers. (e.) Three dimensional rendering of the epileptic foci from different tomographic layers (Movie S2).

the tissue based on compensating the reconstructed image with a pre-calculated optical fluence distribution (Yao et al., 2009; Yuan et al., 2007). It is possible to achieve higher resolution at cellular and even sub-cellular levels to image the neuronal circuitry *in vivo* by use of photoacoustic microscopy at a depth of more than 3 mm (Shelton and Applegate; Hu et al., 2010). The findings imply that PAT has potential for noninvasive real time brain mapping of cortical processing and seizures.

A key advantage of our noninvasive PAT system for epileptiform event monitoring is the real time imaging ability. Seizures are generated by complex interactions of a large group of neurons in which the population of neurons involved varies largely from moment to moment (Schwartz and Bonhoeffer, 2001). By achieving 1000 times

faster data acquisition of the current PAT imaging system relative to our previous PAT system (Zhang et al., 2008), we were able to observe that the spatial aspects of the seizure focus varied over time as suggested by the changes in hemodynamics (Fig. 4c). At present, the imaging speed was limited only by the 10 Hz laser pulse-repetition-rate. Since considerably faster lasers of ~500 Hz pulse-repetition-rates are now commercially available, the temporal resolution of PAT will soon reach a level of a few milliseconds. The light fluence on the skin was less than 5 mJ/cm<sup>2</sup>, well within the American National Standards Institute (Institute, 2007) safety limits. This, coupled with the compactness of an optical system makes it possible to bring a PAT system to the bedside for real time chronic noninvasive monitoring of seizures (Yang et al., 2007).

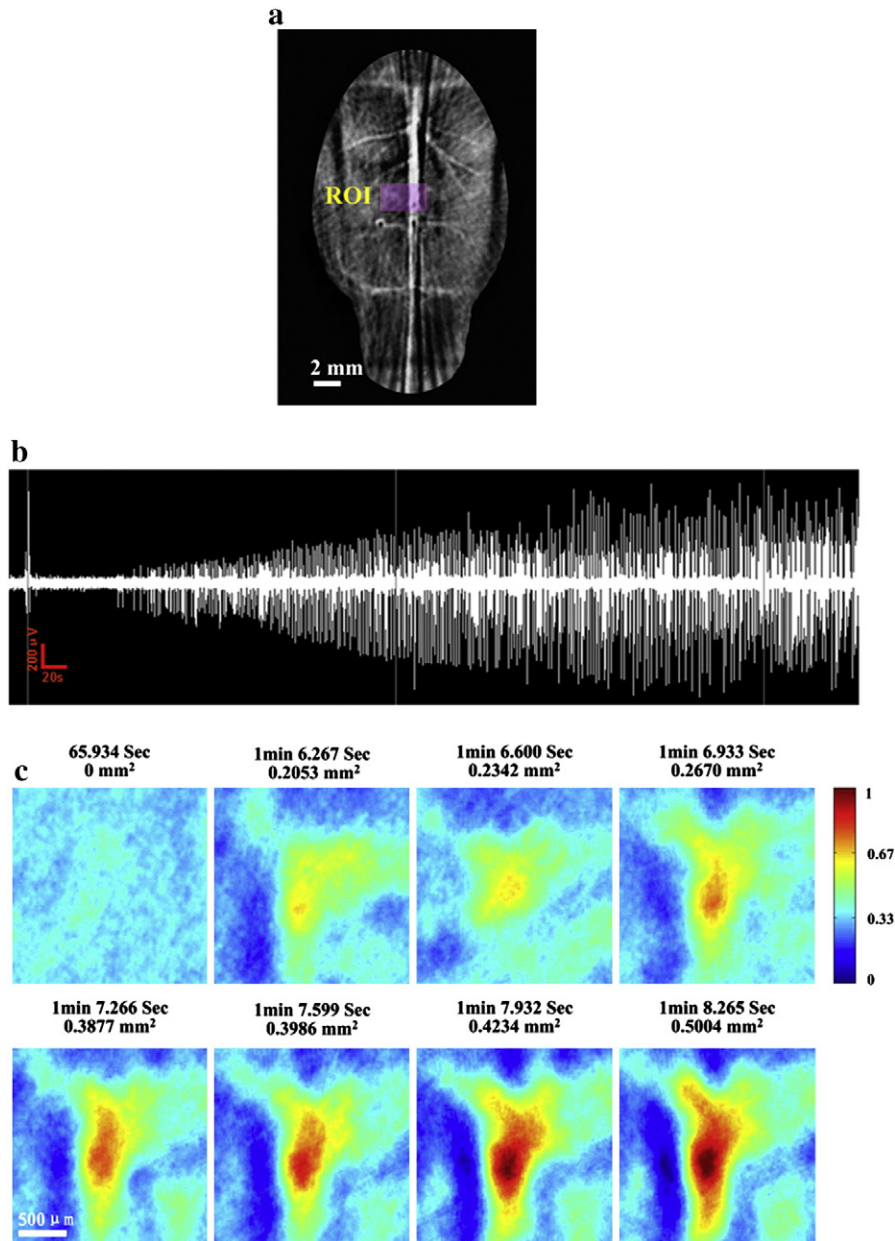


**Fig. 4.** Real-time monitoring of ictal onset. (a.) A PA image showing the cerebral vasculature and the position of BMI injection. ROI, region of interest; Scale bar: 2 mm. (b.) EEG recordings showing the seizure onset about 1 min after BMI injection. (c.) PAT images recording the ictal onset in real time. At 1 min 6.267 s the area of the focus was  $0.2053 \text{ mm}^2$ . The area of the focus then increased in size over the next 2 s to  $0.5004 \text{ mm}^2$ , corresponding to an increase in the amplitude of the EEG spikes. The area of the seizure focus was derived from the PAT images by thresholding to a pixel value one standard deviation above the pixel values from the area of the focus during the control conditions. Scale bar:  $500 \mu\text{m}$  (Movie S3).

One hypothesis is that long-standing epilepsy may lead to the development of secondary epileptogenic regions located at a site distant from the original focus, a factor that may reduce the likelihood of successful epilepsy pre-surgical planning (Cendes et al., 1995). The ability to identify the epileptic focus and associated network may lead to better epilepsy surgery outcomes for many individuals. Various methods such as cross correlation and Granger causality have been explored for assessing the dynamic directional relationships among brain regions using time series data (Bressler et al., 2008; Kaminski et al., 2001). We used Granger causality as a way to quantify the dynamic interactions amongst the primary seizure focus, secondary seizure foci, and middle cerebral artery based on the time-series photoacoustic data. Specifically, Granger causality allowed for assessment of the magnitude and direction of temporal relationships during

overlapping PAT time-series windows. Results further exemplified the temporal aspects of seizure onset, seizure secondary spread, and seizure termination. Collectively, PAT image analysis and tools for effective connectivity may result in a better understanding of epileptic networks at high spatiotemporal resolution.

Little data are available regarding a link between vascular changes and seizures (Nnode-Ekane et al., 2010). We found that the vasomotor phenomena of micro blood vessels correlate with interictal spike and wave discharges (Fig. 6d). Interictal spikes generated a strong cerebral metabolic change that induced cerebral vessel dilation and a focal increase in cerebral blood flow provided oxygenated hemoglobin to hypermetabolic neurons, with a corresponding increase in total hemoglobin (Ma et al., 2009). Vasomotion during seizure onset and spread was clearly caused by the oscillation in vessel diameter

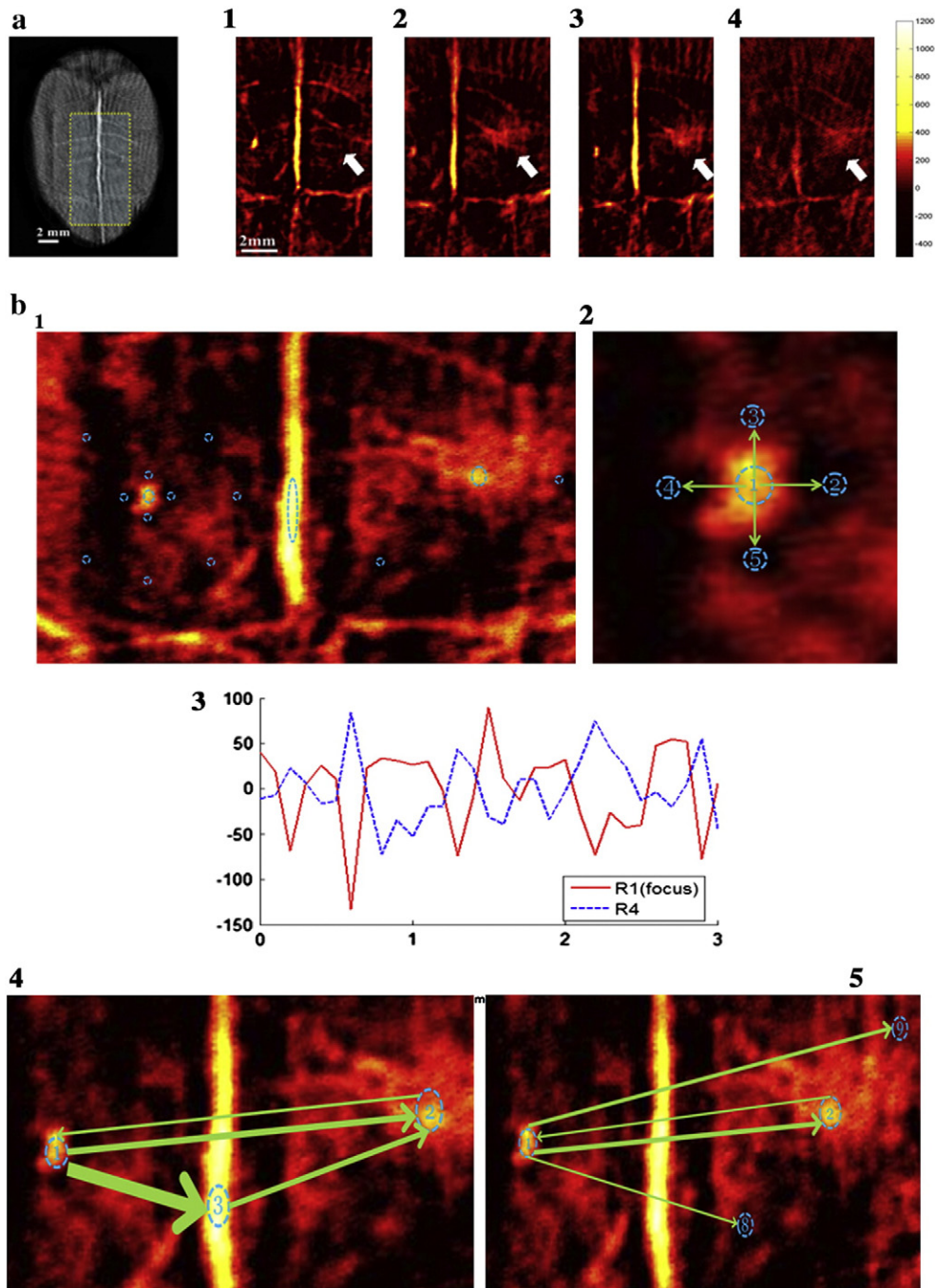


**Fig. 5.** *In vivo* maps of mirror foci propagation. (a.) Left, the PA image of the rat brain; the yellow dotted rectangular shows the ROI for analysis; Right, noninvasive imaging of the primary and mirror foci in bilateral homotopic cortex. a1–4 shows how mirror foci were generated and diminished. White arrow shows the location of mirror foci. The PA signal in the mirror foci was smaller in magnitude and delayed in time compared to the signal recorded from the primary foci. (b.) Granger analysis of seizure foci, mirror foci and middle cerebral artery; b1, a PAT image showing the nine selected ROIs; b2, Granger analysis of the image around the foci and its 'surround' area; b3, PA signal from the foci (red) and surround (blue) during an ictal event. The PA signal surrounding the foci (blue line) shows inverted signal compared to that from the seizure foci (red line) corresponding to neuronal inhibition. b4, connectivity relation between the primary and mirror focus; b5, connectivity relation between the primary focus, mirror focus and middle cerebral artery. The line width stands for the relative Granger causal influence strength.

and the expansion of the vessel cross section. We reasoned that the dilation resulted in an active cerebral microvasculature response to increased metabolic activity accompanying the seizure (Myers and Intaglietta, 1976). The combination of multi-scale imaging ability and endogenous hemoglobin contrast makes PAT a promising tool for imaging microvasculature during seizure onset. Future quantitative PAT studies will allow us to resolve many of the hemodynamic components, including changes in level of hemoglobin oxygenation (i.e., deoxy- and

oxy-hemoglobin), cerebral blood flow, and the rate of cerebral oxygen metabolism, for a detailed understanding of the neurovascular coupling phenomenon, both during and in between seizures (Yao et al., 2009; Yuan et al., 2007).

The present work represents a major technological and scientific improvement in epilepsy. Previous attempts to track from moment to moment populations of neurons participating in an epileptiform event had not been possible with any technique or tool because of

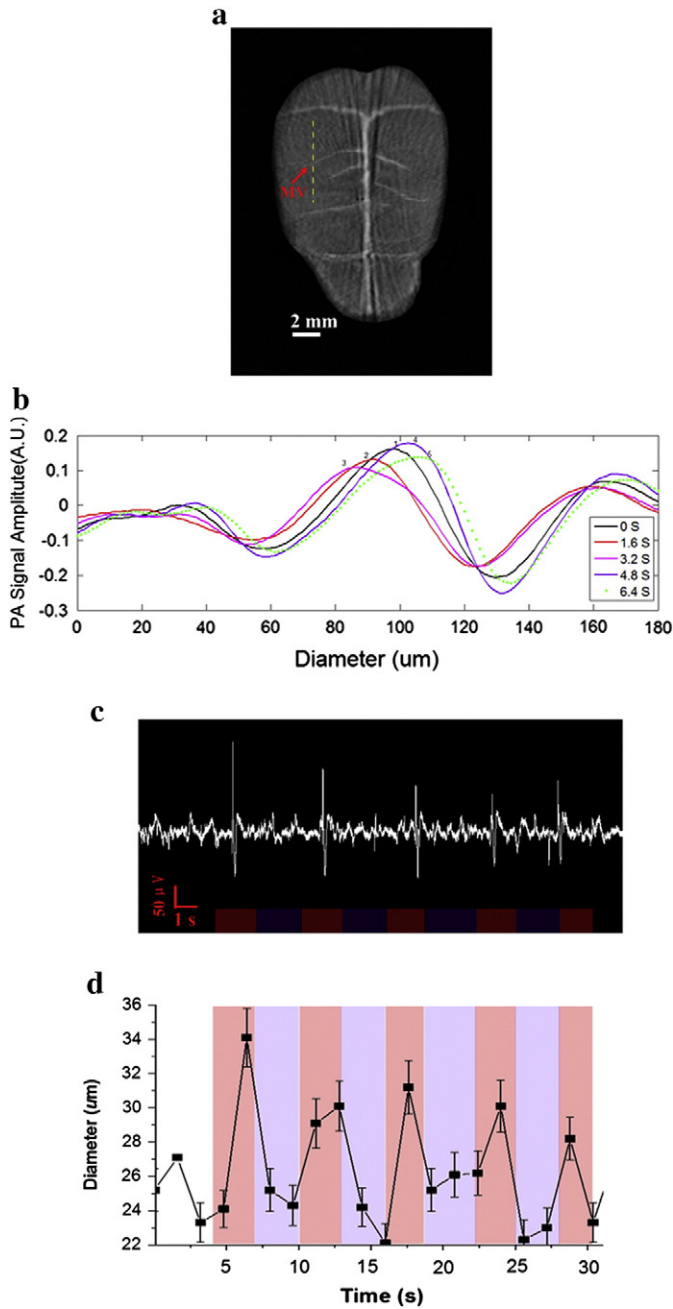


**Fig. 6.** Changes of blood vessel diameter during interictal onset. (a.) PA image of the rat cortex vasculature with the intact scalp and skull. The red arrow indicates the microvasculature (MV) along the yellow dashed line direction for a cross-sectional scanning using a 50 MHz ultrasound transducer. (b.) Typical photoacoustic signals from the targeted vessel at different times. (c.) EEG recordings show the interictal spikes and (d.) Change of the vessel size captured by PAT. Here was a clear correlation between the interictal spikes and the changes of the vessel size. Error bars ( $\pm$ s.d.) were calculated from 20 consecutive spikes.

spatial and/or temporal sampling limitations. The high spatial and temporal sampling of the novel PAT system allowed for the first time the complete mapping of an epileptiform event *in vivo*. Another major improvement is that this is the first report of mapping an epileptiform event at depths well below the cortex. In terms of impact, this is the first demonstration of emerging optical mapping tool in the surgical evaluation of focal cortical epilepsy, since accurate localization of the epileptic focus, propagation paths, and subcortical networks critically depends on the precise localization of epileptogenic neurons and networks. The use of our PAT system, experimental

paradigm, results, and analyses advances our understanding of epilepsy and seizure temporal spatial properties relative to previous attempts. The noninvasive yet whole surface and depth capabilities of the PAT system allowed for the first time to actually see what is happening during ictogenesis in terms of seizure onset and spread. The challenge of mapping focal epilepsy stems from the observation that the pathology associated with focal epilepsy is often distributed across a number of brain sites. Seizures in animal models and in people often have a multifocal or broadly synchronized onset. The implication of these observations is that each of the sites could act independently to initiate a seizure or, potentially, to drive another site into a seizure. The current study lends support to the theory that seizure onset and spread involves a rich interplay between multiple cortical and subcortical foci during the onset and spread of focal epilepsy. The findings are timely in the sense that the neuroscience community is questioning the long-held dogma that seizure onset involves some sort of single focus or epicenter in favor of the emerging thought that seizures instead involve multiple cortical and subcortical foci.

### Acknowledgments

This research was supported in part by a grant from the US Department of Defense Congressionally Directed Medical Program, the B.J. and Eve Wilder endowment fund, and the Children's Miracle Network.

### Appendix A. Supplementary data

Supplementary data to this article can be found online at <http://dx.doi.org/10.1016/j.neuroimage.2012.10.077>.

### Reference

- Berg, A.T., Langfitt, J.T., Spencer, S.S., Vickrey, B.G., 2007. Stopping antiepileptic drugs after epilepsy surgery: a survey of U.S. epilepsy center neurologists. *Epilepsy Behav.* 10, 219–222.
- Bertram, E.H., 2009. Temporal lobe epilepsy: where do the seizures really begin? *Epilepsy Behav.* 14, 32–37.
- Bertram, E.H., Zhang, D.X., Mangan, P., Fountain, N., Rempe, D., 1998. Functional anatomy of limbic epilepsy: a proposal for central synchronization of a diffusely hyperexcitable network. *Epilepsy Res.* 32, 194–205.
- Birbeck, G.L., Hays, R.D., Cui, X., Vickrey, B.G., 2002. Seizure reduction and quality of life improvements in people with epilepsy. *Epilepsia* 43, 535–538.
- Bluestone, A.Y., Abdoulaev, G., Schmitz, C.H., Barbour, R.L., Hielscher, A.H., 2001. Three-dimensional optical tomography of hemodynamics in the human head. *Opt. Express* 9, 272–286.
- Boas, D.A., Gaudette, T., Strangman, G., Cheng, X., Marota, J.J., Mandeville, J.B., 2001. The accuracy of near infrared spectroscopy and imaging during focal changes in cerebral hemodynamics. *Neuroimage* 13, 76–90.
- Bressler, S.L., Tang, W., Sylvester, C.M., Shulman, G.L., Corbetta, M., 2008. Top-down control of human visual cortex by frontal and parietal cortex in anticipatory visual spatial attention. *J. Neurosci.* 28, 10056–10061.
- Brovelli, A., Ding, M., Ledberg, A., Chen, Y., Nakamura, R., Bressler, S.L., 2004. Beta oscillations in a large-scale sensorimotor cortical network: directional influences revealed by Granger causality. *Proc. Natl. Acad. Sci. U. S. A.* 101, 9849–9854.
- Cadotte, A.J., DeMarse, T.B., Mareci, T.H., Parekh, M.B., Talathi, S.S., Hwang, D.U., Ditto, W.L., Ding, M.Z., Carney, P.R., 2010. Granger causality relationships between local field potentials in an animal model of temporal lobe epilepsy. *J. Neurosci. Methods* 189, 121–129.
- Cendes, F., Cook, M.J., Watson, C., Andermann, F., Fish, D.R., Shorvon, S.D., Bergin, P., Free, S., Dubeau, F., Arnold, D.L., 1995. Frequency and characteristics of dual pathology in patients with lesional epilepsy. *Neurology* 45, 2058–2064.
- Denk, W., Strickler, J.H., Webb, W.W., 1990. Two-photon laser scanning fluorescence microscopy. *Science* 248, 73–76.
- Duncan, J.S., Sander, J.W., Sisodiya, S.M., Walker, M.C., 2006. Adult epilepsy. *Lancet* 367, 1087–1100.
- Engel, J., 2004. The goal of epilepsy therapy: no seizures, no side effects, as soon as possible. *CNS Spectr.* 9, 95–97.
- Folbergrová, J., Ingvar, M., Siesjö, B.K., 1981. Metabolic changes in cerebral cortex, hippocampus, and cerebellum during sustained bicuculline-induced seizures. *J. Neurochem.* 37, 1228–1238.
- Fountain, N.B., Bear, J., Bertram, E.H., Lothman, E.W., 1998. Responses of deep entorhinal cortex are epileptiform in an electrogenic rat model of chronic temporal lobe epilepsy. *J. Neurophysiol.* 80, 230–240.
- Granger, C.W.J., 1969. Investigating causal relations by econometric models and cross-spectral methods. *Econometrica* 37 (414–8).

- Greenfield, J., Geyer, J., Carney, P.R., 2011. Reading EEGs: a Practical Approach. Lippincott Wilkins Raven, Philadelphia.
- Grinvald, A., Frostig, R.D., Lieke, E., Hildesheim, R., 1988. Optical imaging of neuronal activity. *Physiol. Rev.* 68, 1285–1366.
- Haglund, M.M., Hochman, D.W., 2004. Optical imaging of epileptiform activity in human neocortex. *Epilepsia* 45, 43–47.
- Haglund, M.M., Ojemann, G.A., Hochman, D.W., 1992. Optical imaging of epileptiform and functional activity in human cerebral cortex. *Nature* 358, 668–671.
- Hauser, W.A., 1992. Seizure disorders: the changes with age. *Epilepsia* 33 (Suppl. 4), S6–14.
- Hauser, W.A., Annegers, J.F., Rocca, W.A., 1996. Descriptive epidemiology of epilepsy: contributions of population-based studies from Rochester, Minnesota. *Mayo Clin. Proc.* 71, 576–586.
- Hill, D.K., Keynes, R.D., 1949. Opacity changes in stimulated nerve. *J. Physiol. (Lond.)* 108, 278–281.
- Hu, S., Rao, B., Maslov, K., Wang, L.V., 2010. Label-free photoacoustic ophthalmic angiography. *Opt. Lett.* 35, 1–3.
- Huang, D., Swanson, E.A., Lin, C.P., Schuman, J.S., Stinson, W.G., Chang, W., Hee, M.R., Flotte, T., Gregory, K., Puliafito, C.A., Fujimoto, J.G., 1991. Optical coherence tomography. *Science* 254, 1178–1181.
- Institute, A.N.S., 2007. American national standard for the safe use of lasers. ANSI z136.1. Laser Institute of America, Orlando, Fla.
- Jeha, L.E., Najm, I., Bingaman, W., Dinner, D., Widdess-Walsh, P., Luders, H., 2007. Surgical outcome and prognostic factors of frontal lobe epilepsy surgery. *Brain* 130, 574–584.
- Jiang, H.B., Paulsen, K.D., Osterberg, U.L., Pogue, B.W., Patterson, M.S., 1996. Optical image reconstruction using frequency-domain data: simulations and experiments. *J. Opt. Soc. Am. A* 13, 253–266.
- Kaminski, M., Ding, M.Z., Truccolo, W.A., Bressler, S.L., 2001. Evaluating causal relations in neural systems: Granger causality, directed transfer function and statistical assessment of significance. *Biol. Cybern.* 85, 145–157.
- Khalilov, I., Holmes, G.L., Ben-Ari, Y., 2003. In vitro formation of a secondary epileptogenic mirror focus by interhippocampal propagation of seizures. *Nat. Neurosci.* 6, 1079–1085.
- Kruger, R.A., Liu, P.Y., 1994. Photoacoustic ultrasound — pulse production and detection in 0.5-percent liposyn. *Med. Phys.* 21, 1179–1184.
- Laufer, J., Delpy, D., Elwell, C., Beard, P., 2007. Quantitative spatially resolved measurement of tissue chromophore concentrations using photoacoustic spectroscopy: application to the measurement of blood oxygenation and haemoglobin concentration. *Phys. Med. Biol.* 52, 141–168.
- Ma, H., Zhao, M., Suh, M., Schwartz, T.H., 2009. Hemodynamic surrogates for excitatory membrane potential change during interictal epileptiform events in rat neocortex. *J. Neurophysiol.* 101, 2550–2562.
- Mace, E., Montaldo, G., Cohen, I., Baulac, M., Fink, M., Tanter, M., 2011. Functional ultrasound imaging of the brain. *Nat. Methods* 8, 662–U685.
- Mangan, P.S., Scott, C.A., Williamson, J.M., Bertram, E.H., 2000. Aberrant neuronal physiology in the basal nucleus of the amygdala in a model of chronic limbic epilepsy. *Neuroscience* 101, 377–391.
- Myers, R.R., Intaglietta, M., 1976. Brain microvascular hemodynamic responses to induced seizures. *Stroke* 7, 83–88.
- Ndode-Ekane, X.E., Hayward, N., Grohn, O., Pitkanen, A., 2010. Vascular changes in epilepsy: functional consequences and association with network plasticity in pilocarpine-induced experimental epilepsy. *Neuroscience* 166, 312–332.
- Ogawa, S., Lee, T.M., Nayak, A.S., Glynn, P., 1990. Oxygenation-sensitive contrast in magnetic-resonance image of rodent brain at high magnetic-fields. *Magn. Reson. Med.* 14, 68–78.
- Oleary, M.A., Boas, D.A., Chance, B., Yodh, A.G., 1995. Experimental images of heterogeneous turbid media by frequency-domain diffusing-photon tomography. *Opt. Lett.* 20, 426–428.
- Paxinos, G.W.C., 1998. *The Rat Brain*. Academic Press.
- Schwartz, T.H., Bonhoeffer, T., 2001. *In vivo* optical mapping of epileptic foci and surround inhibition in ferret cerebral cortex. *Nat. Med.* 7, 1063–1067.
- Shelton, R.L., Applegate, B.E., 2010. Ultrahigh resolution photoacoustic microscopy via transient absorption. *Biomed. Opt. Express* 1, 676–686.
- Sipkins, D.A., Wei, X.B., Wu, J.W., Runnels, J.M., Cote, D., Means, T.K., Luster, A.D., Scadden, D.T., Lin, C.P., 2005. In vivo imaging of specialized bone marrow endothelial microdomains for tumour engraftment. *Nature* 435, 969–973.
- Sokol, D.K., Markand, O.N., Daly, E.C., Luerssen, T.G., Malkoff, M.D., 2000. Near infrared spectroscopy (NIRS) distinguishes seizure types. *Seizure* 9, 323–327.
- Steinhoff, B.J., Herrendorf, G., Kurth, C., 1996. Ictal near infrared spectroscopy in temporal lobe epilepsy: a pilot study. *Seizure* 5, 97–101.
- Thom, M., Mathem, G.W., Cross, J.H., Bertram, E.H., 2010a. Mesial temporal lobe epilepsy: how do we improve surgical outcome? *Ann. Neurol.* 68, 424–434.
- Thom, M., Mathern, G.W., Cross, J.H., Bertram, E.H., 2010b. Mesial temporal lobe epilepsy: how do we improve surgical outcome? *Ann. Neurol.* 68, 424–434.
- Wang, X., Chen, Y.H., Bressler, S.L., Ding, M.Z., 2007. Granger causality between multiple interdependent neurobiological time series: blockwise versus pairwise methods. *Int. J. Neural Syst.* 17, 71–78.
- Watanabe, E., Maki, A., Kawaguchi, F., Yamashita, Y., Koizumi, H., Mayanagi, Y., 2000. Noninvasive cerebral blood volume measurement during seizures using multichannel near infrared spectroscopic topography. *J. Biomed. Opt.* 5, 287–290.
- Xiang, L.Z., Xing, D., Gu, H.M., Yang, D.W., Yang, S.H., Zeng, L.M., Chen, W.R., 2007. Real-time photoacoustic monitoring of vascular damage during photodynamic therapy treatment of tumor. *J. Biomed. Opt.* 12.
- Yang, S.H., Xing, D., Lao, Y.Q., Yang, D.W., Zeng, L.M., Xiang, L.Z., Chen, W.R., 2007. Non-invasive monitoring of traumatic brain injury and post-traumatic rehabilitation with laser-induced photoacoustic imaging. *Appl. Phys. Lett.* 90.
- Yao, L., Sun, Y., Jiang, H.B., 2009. Quantitative photoacoustic tomography based on the radiative transfer equation. *Opt. Lett.* 34, 1765–1767.
- Yuan, Z., Wang, Q., Jiang, H.B., 2007. Reconstruction of optical absorption coefficient maps of heterogeneous media by photoacoustic tomography coupled with diffusion equation based regularized Newton method. *Opt. Express* 15, 18076–18081.
- Zhang, Q.Z., Liu, Z., Carney, P.R., Yuan, Z., Chen, H.X., Roper, S.N., Jiang, H.B., 2008. Non-invasive imaging of epileptic seizures in vivo using photoacoustic tomography. *Phys. Med. Biol.* 53, 1921–1931.